Waves in Diffusively Coupled Bursting Cells

Sridhar Raghavachari and James A. Glazier
Department of Physics, University of Notre Dame, Notre Dame, Indiana 46556
(Received 20 May 1998)

We analyze the dynamics of a spatially extended system with bistability between a homogeneous stationary state and an unstable fixed point surrounded by an oscillatory state. We show that a wave front extinguishes homogeneous oscillations, replacing them with unsteady oscillations. A traveling wave solution connects the unsteady oscillations to the stationary state. The difference in potentials of the fixed points alone determines the velocity of the wave-front fixed points. We apply our results to a generic model of neuronal bursting. [S0031-9007(99)08785-2]

PACS numbers: 87.16.–b, 02.60.Lj, 05.45.–a, 87.10.+e

Bursting characterizes a variety of biological oscillators [1]. Typically, the electrical potential of a bursting cell undergoes a succession of alternating active and silent phases. In the active phase, the membrane potential oscillates rapidly, and in the silent phase, it evolves slowly without oscillations. Single cell models of bursting consist of a set of ordinary differential equations governing the behavior of the fast variable and at least one slow variable. The presence of a slow variable in single cell models allows us to take the singular limit, to decompose the activity into a fast subsystem which treats the slow variables as parameters, and a slow subsystem [2]. Models with a single slow variable S burst when the fast subsystem is bistable between a low voltage rest state and high voltage oscillations for a range of values of S. As the slow variable evolves, the trajectory exhibits hysteresis between the silent phase and the active phase oscillations.

Several models describe the activity of single cells in various situations, but the study of coupled bursters is incomplete. We consider a model from neurobiology [3] that exhibits bursting oscillations and study the dynamics of a field of bursters with a weak resistive coupling between neighboring cells. This situation arises in the study of bursting activity in the β-cell islets of the pancreas, which secrete insulin in response to glucose in the blood. Experimental measurements of the coupling strengths between cells [4], which indicate that the coupling is weak, raise the following questions: Does the spatially extended model still exhibit well-defined bursts; i.e., does the whole domain synchronously switch between active and silent phases? Note that oscillations within the burst need not be synchronous. A recent study [5] of a model with a similar phase portrait shows strong spatiotemporal intermittency. Does intermittency occur in a model of diffusively coupled bursters as well? If so, and if the gap junction coupling is indeed weak, pancreatic islets should secrete in chaotic bursts, which would have physiologically disastrous consequences. We answer these questions for a minimal (generic) model for bursting, using singular perturbation theory and techniques developed for reaction-diffusion equations.

The Hindmarsh-Rose equations [3] are a simple polynomial model of bursting in thalamic cells, which capture certain generic features of more complicated biophysical models. The equations for a continuum coupled Hindmarsh-Rose model are

$$v_t = w + 3v^2 - v^3 - \mu + Dv_{xx}\,, \tag{1}$$

$$w_t = 1 - 5v^2 - w\,, \tag{2}$$

$$\mu_t = \epsilon\left(v - \frac{(\mu - z)}{4}\right), \tag{3}$$

where v is the voltage, w is a recovery variable, D is the strength of diffusive coupling, μ is a slow variable, and z is a slow subsystem parameter that controls the nature of bursting. In order to understand the behavior of Eqs. (1)–(3), we first take the singular limit $\epsilon \to 0$, $\mu(x) = \mu$, which results in a planar reaction-diffusion equation. The dynamics on this fast subspace then carry over to the full model when ϵ is nonzero.

We conveniently write Eqs. (1) and (2) in a Liénard form, i.e., as a nonlinear oscillator with a small damping term. The governing equations then become

$$v_{tt} + G(v,\mu) + F(v)v_t = Dv_{xx} + Dv_{xxt}\,, \tag{4}$$

where $G(v,\mu) = v^3 + 2v^2 + \mu - 1$, which can be considered as the gradient of a potential $V(v,\mu)$, and a damping term $F(v) = 1 + 3v^2 - 6v$. The roots of $G(v,\mu)$ give the fixed points of the equations, which typically have either one or three real roots depending on the parameter μ.

We show the bifurcation diagram of Eqs. (1) and (2) as a function of μ in Fig. 1 (we compute all bifurcation diagrams using the bifurcation software AUTO [6]). The upper branch of steady states loses stability by a Hopf bifurcation at $\mu \sim -11.5$. At $\mu \sim -0.1815$, a saddle-node bifurcation creates two additional steady state branches (middle: saddle; lower: sink). As μ increases, the amplitude of the periodic orbit increases until it disappears through an Andronov homoclinic bifurcation at $\mu^* \sim 0.8$. Bistable behavior is common, with examples from biology, chemical

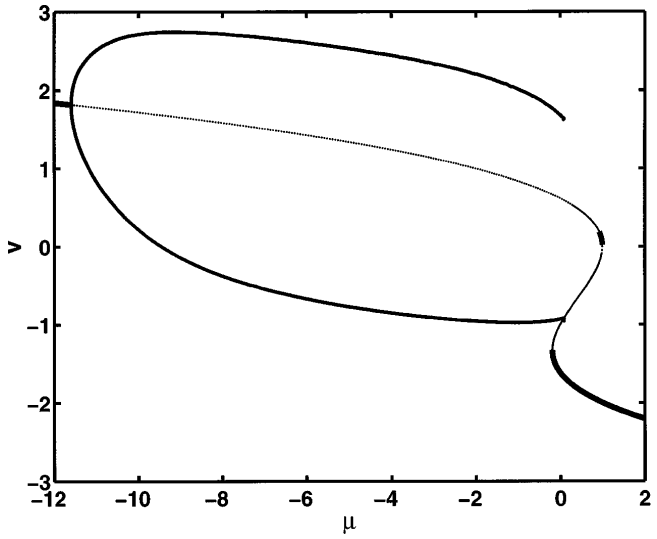

FIG. 1. Bifurcation diagram for the Hindmarsh-Rose equations. Heavy lines indicate stable fixed points and thin lines indicate unstable fixed points. The equations have another Hopf bifurcation at $\mu \sim 0.8$ which terminates in a homoclinic bifurcation nearby, but these bifurcations play no role in bursting or front propagation.

reactions, and models of fluid dynamics [7,8]. We restrict our attention to values of μ, where Eqs. (1) and (2) are bistable between a sink and a limit cycle. We label the three equilibria as the unstable fixed point (UFP) (unstable focus) surrounded by the stable limit cycle, a SP (saddle point), and the lower fixed point (LFP) (sink).

We consider the homogeneous oscillations (the active phase for bursting) that emerge from the Hopf bifurcation of the UFP. With nonzero coupling, the periodic orbit loses stability to localized perturbations. In Fig. 2, we show a numerical integration of the reaction-diffusion equations (we reduce the partial differential equations to a set of ordinary differential equations by finite difference and use Gear's method [9] for integration for all of the numerical integrations). Initial conditions are homogeneous oscillations, with a small phaselike perturbation at the left end. The perturbation grows and moves into the oscillating regime, leaving behind a region of unsteady oscillations.

We give a qualitative explanation of the origin of the unsteady oscillations by an analysis similar to [10], and examine the dynamics of the front in a later publication. Although the coupling is only in v, the oscillators can differ in both v and w along the limit cycle. The SP deforms the phase flow along the periodic orbit. If the trajectories of two interacting oscillators are close to the limit cycle, but their phases are different, the interaction drives them away from the limit cycle. The lagging oscillator is pushed out and slows down as it travels along the stable manifold of the saddle point. The leading oscillator is pushed in and departs from the limit cycle. Away from the saddle point, the limit cycle attracts nearby points and synchronizes the oscillators. The phase portrait [a plot of $v(x)$ versus $w(x)$] for any location behind the front is dense and completely fills the region bounded by the phase portrait of the periodic orbit of the diffusionless equations. The above approach is valid if the diffusive term is sufficiently weak [11] (more precisely, if the diffusive term does not perturb the limit cycle), which is the case we consider.

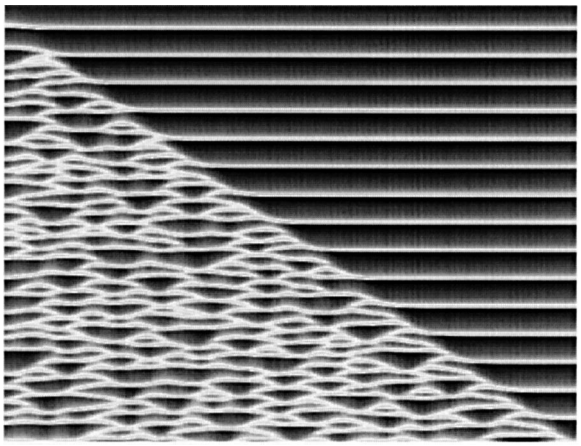

FIG. 2. Numerical integration of Eqs. (1) and (2). Light and dark regions indicate high and low values of the variable v. Length is 40 units and total time is 200 units. Space increases from left to right and time from top to bottom. D is 0.2 and μ is set to -0.15. The front separating the unsteady oscillations from the homogeneous oscillations moves with a velocity of approximately 0.2.

Figure 3 shows the numerical integration of the equations, with the initial conditions set at the LFP, with a small patch excited close to the UFP. We see a front advancing to the right with a constant velocity, leaving behind a region of unstable oscillations, much like the ones observed in the case of the propagation of a phaselike disturbance into the homogeneously oscillating region. A uniform state

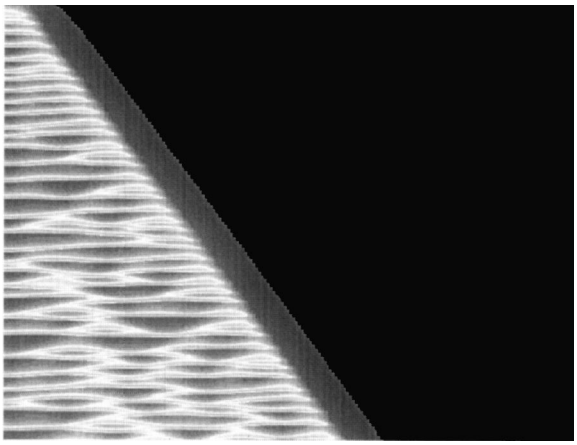

FIG. 3. Numerical integration of Eqs. (1) and (2). Light and dark regions are as in Fig. 2. Space increases from left to right and time from top to bottom. Grid size is 200, with domain length of 20. Total time is 200 units. D and μ are the same as for Fig. 2. The initial conditions are mentioned in the text. The front velocity is approximately 0.055 which is close to the value obtained from the perturbation analysis.

corresponding to UFP cannot be established since this state is unstable for the original reaction equations. A modulated oscillatory state is also ruled out since the wave-number selection by the front competes with the dephasing interaction and renders the oscillations unstable. Therefore, the front leaves behind a region of irregular oscillations.

Instability of the homogeneous oscillations suggests that we approximate the front connecting the unsteady oscillations by the front between the UFP and the LFP instead. The potential $V(v, \mu)$ has two minima at the UFP. For $\mu < \mu^*$, $V(\mathrm{LFP}, \mu) < V(\mathrm{UFP}, \mu)$ indicating that the front switches the domain from the metastable state to the stable state, and the front velocity is positive. A front solution is a stationary solution in the moving frame, $\{v(\xi), w(\xi)\}$, with $\xi = x - ct$, and $c > 0$. The equations now become

$$x_1' = x_2\,, \tag{5}$$

$$x_2' = x_3\,, \tag{6}$$

$$Dcx_3' = -G(x_1, \mu) + cF(x_1)x_2 + (D - c^2)x_3\,, \tag{7}$$

where $'$ denotes $\frac{d}{d\xi}$, and $x_1 = v$, $x_2 = v_\xi$, and $x_3 = v_{\xi\xi}$.

We use a numerical shooting method to compute the velocity of the front as a function of μ, using Gear's method for numerical integration of the equations [9], and show the dependence of c on μ in Fig. 4. The front speed tends to 0 near the Maxwell point (the value of μ where the potentials of the two steady states are equal).

We also computed the velocity of the front separating the LFP from unsteady oscillations by a simple perturbation analysis of the stationary front connecting the UFP and the LFP. Numerical computations show that the front velocity is rather small, suggesting that we use c as a small parameter, with the singular limit $c = 0$. Setting $c = 0$, $\mu = \mu_M$ in Eqs. (5)–(7) gives us the stationary front solution (μ_M being the value of μ where the potentials are equal),

$$x_1(\xi) = a[1 + \exp(-a\xi\sqrt{5}/\sqrt{2})] - b\,, \tag{8}$$

where a and b are constants. For μ close to μ_M, a solvability condition, following standard perturbation techniques, determines the front velocity, $c \sim 0.092(\mu_M - \mu)$, which agrees with the average velocity of the front computed from the direct numerical integration of Eqs. (5)–(7) (not shown), indicating that only the difference in potential of the two fixed points determines the front velocity. The front velocity computed using the shooting method is approximate (Fig. 4), and agrees with the velocity computed using the perturbation method, for $\mu > \mu^*$, where μ^* is the homoclinic point.

We can now apply the results obtained for the fast subsystem to study a field of diffusively coupled bursters. The Hindmarsh-Rose equations have a bursting solution known as square wave bursting from the shape of the burst envelope. Pernarowski [12] studied a polynomial model of coupled bursting cells distributed on the unit interval with strong coupling and has shown that for certain initial conditions, the model tends to burst uniformly. However, as we show below, weak coupling results in very different behavior. We set $D = 0.2$ to denote weak diffusion, although the results are qualitatively the same as long as $D \ll \frac{1}{\epsilon}$. The front speeds increase as $\sqrt{D}$ [13], but the existence and stability of the fronts are unchanged.

Figure 5 shows the bifurcation diagram of the fast subsystem with the nullcline of the slow subsystem superimposed, along with the phase portrait of the bursting

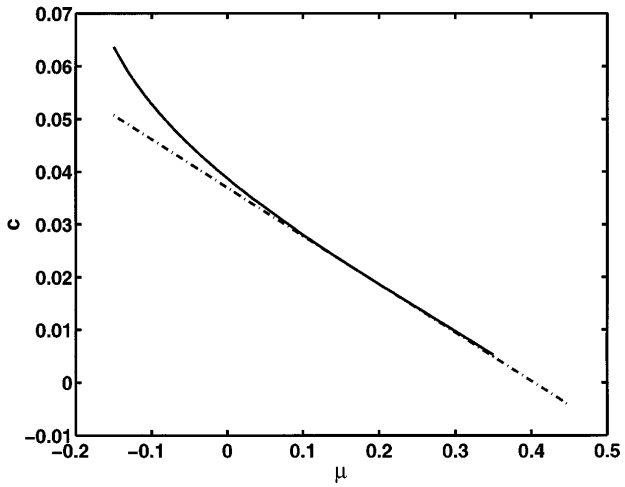

FIG. 4. Variation of front velocity with the parameter μ. The broken line is calculated from the perturbation analysis and the full line is the velocity calculated using the shooting method.

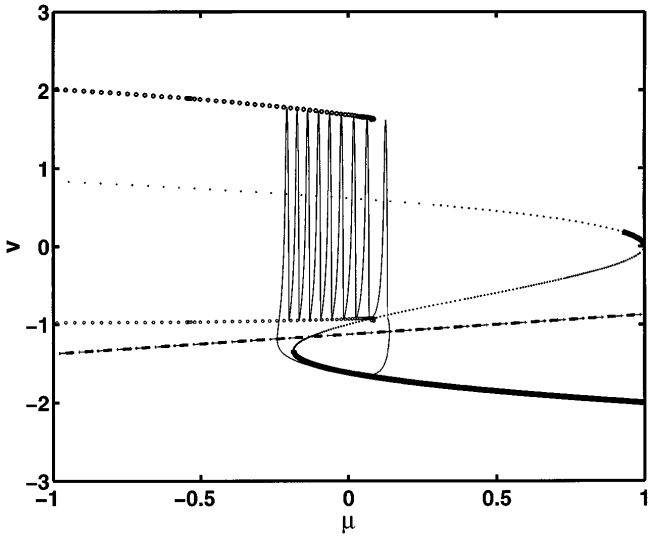

FIG. 5. Numerical solution of the full Hindmarsh-Rose equations (with $D = 0$) projected onto the fast subsystem bifurcation diagram. The dot-dashed line is the μ nullcline. Heavy lines indicate stable steady states and thin lines indicate unstable steady states. Open circles represent stable periodic orbits. The silent phase tracks the lower branch of steady states and is excited into the active phase near the saddle-node point. The active phase tracks the periodic orbit of the fast subsystem and terminates at the homoclinic orbit.

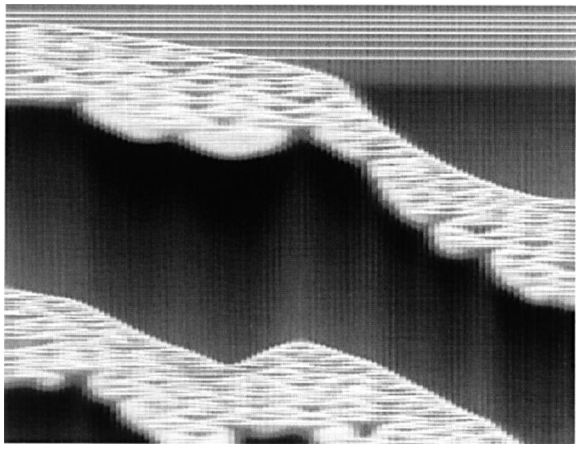

FIG. 6. Numerical integration of Eqs. (1)–(3) with $D = 0.2$. v is indicated by light and dark regions as in Fig. 2. System length is 20, increasing from left to right, and the total time is 1000, increasing from top to bottom. A spatial wave of bursting spreads across the system.

oscillations. The slow subsystem parameter z controls the nature of bursting in the full model [14]. For $z = 4.5$, the single cell bursts with nine spikes. We show the evolution of the full model in Fig. 6. The entire domain is set in the active phase with a small patch at the left end advanced in phase along the active phase oscillation. A wave of bursting sweeps across the domain with well-defined active and silent phases, but the oscillations in the active phase are now irregular and the bursting does not terminate at the same value of μ for all x. The burst period is also larger than for the single cell model. A well-defined wave front separates the bursting region from the silent region. A second, irregular wave front switches the domain from the active to the silent phase.

A phase portrait for $x = 10$ shows that the irregular oscillations persist for $\mu > \mu^*$, strongly suggesting that the homoclinic bifurcation no longer plays a role in burst termination. Instead, the active phase continues until μ reaches μ_M and the upper and middle branches in Fig. 1 disappear in a saddle-node bifurcation, leaving the lower fixed point as the only stationary state. Then μ begins to decrease, since v switches below the μ nullcline (Fig. 5). Since $\mu > \mu_M$, a (locally well-defined) front develops with the steady state replacing the oscillations to the right and the active phase terminates. These observations suggest that diffusively coupled bursters do not have regular active phase oscillations nor do they burst homogeneously.

In conclusion, a continuum model of bursters, coupled by weak electrical coupling, does not burst uniformly with well-defined active phase oscillations. This result suggsts that synchronous bursting in the intact pancreatic islet requires strong coupling. Moreover, the nucleation driven chaos found in [5] does not occur in generic models of bursting. Simulations of other model equations, with both polynomial and more complex kinetics for the fast subsystems, show that the above behavior is generic. Since the Hindmarsh-Rose equations are closely related to the normal form for a codimension-3 Takens-Bogdanov bifurcation [15], which is the topological model for the fast subsystems of most types of bursters [16], our results apply to more general models of square wave bursters including other bursters constructed from this codimension-3 normal form.

This research was supported by the NSF/NYI DMR-9257011 and the American Chemical Society/Petroleum Research Fund.

[1] J. Rinzel and X-J. Wang in *Handbook of Neural Networks and Brain Function*, edited by M. Arbib (MIT Press, Cambridge, MA, 1995), p. 687–691.
[2] J. Rinzel and Y. Lee in *Nonlinear Oscillations in Biology and Chemistry*, edited by H. Othmer (Springer-Verlag, New York, 1986).
[3] J. L. Hindmarsh and R. M. Rose, Proc. R. Soc. London B **221**, 87 (1984).
[4] M. Perez-Armandriz, M. C. Roy, D. C. Spray, and M. V. L. Bennett, Biophys. J. **59**, 76 (1991).
[5] M. Argentina and P. Coullet, Phys. Rev. E **56**, R2359 (1997).
[6] E. Doedel, Cong. Num. **30**, 265 (1981).
[7] *Oscillations and Traveling Waves in Chemical Systems*, edited by R. J. Field and M. Burger (John Wiley, New York, 1985).
[8] M. C. Cross and P. C. Hohenberg, Rev. Mod. Phys. **65**, 2 (1993).
[9] C. W. Gear, Math. Comput. **21**, 146 (1967).
[10] S. K. Han, C. Kurrer, and Y. Kuramoto, Phys. Rev. Lett. **75**, 3190 (1995).
[11] Y. Kuramoto, *Chemical Oscillations, Waves and Turbulence* (Springer-Verlag, Berlin, 1984).
[12] M. Pernarowski, SIAM J. Appl. Math. (to be published).
[13] G. A. Klaasen and W. C. Troy, SIAM J. Appl. Math. **41**, 145 (1981).
[14] X-J. Wang, Physica (Amsterdam) **62D**, 263 (1993).
[15] F. Dumortier, R. Roussarie, J. Sotomayor, and H. Zoladek, *Bifurcations of Planar Vector Fields: Nilpotent Singularities and Abelian Integrals*, Lecture Notes in Mathematics (Springer-Verlag, Berlin, 1991), Vol. 1480.
[16] R. Bertram, M. J. Butte, T. Kiemel, and A. Sherman, Bull. Math. Biol. **57**, 413 (1995).